Journal of Power Sources 239 (2013) 466–474

Contents lists available at SciVerse ScienceDirect

Journal of Power Sources

journal homepage: www.elsevier.com/locate/jpowsour

A facile synthesis of Fe_3O_4/C composite with high cycle stability as anode material for lithium-ion batteries

Peng Wang, Mingxia Gao*, Hongge Pan*, Jialei Zhang, Chu Liang, Junhua Wang, Pei Zhou, Yongfeng Liu

State Key Laboratory of Silicon Materials, Key Laboratory of Advanced Materials and Applications for Batteries of Zhejiang Province & Department of Materials Science and Engineering, Zhejiang University, Hangzhou 310027, P.R.China

HIGHLIGHTS

- Fe_3O_4/C composites are synthesized from Fe_2O_3/acetylene black by carbothermal reduction.
- Fe_3O_4 particles inherit the nano-size feature of Fe_2O_3 and are well dispersed in the composite.
- Fe_3O_4/C composites with sufficient carbon provide superior electrochemical performance.
- The method is facile in large-scale production of anode material for lithium-ion batteries.

ARTICLE INFO

Article history:
Received 16 January 2013
Received in revised form
25 February 2013
Accepted 10 March 2013
Available online 6 April 2013

Keywords:
Lithium-ion batteries
Anode
Reduction
Iron oxides
Acetylene black
Electrochemical performance

ABSTRACT

Fe_3O_4/C composites are synthesized by ball milling nano-sized Fe_2O_3 powder with acetylene black (AB) in different ratios followed by a carbothermal reduction at 600 °C for 6 h. Structural evolution of the Fe_2O_3/AB mixtures during the carbothermal reduction and the electrochemical properties of the Fe_3O_4/C composites as anode materials for lithium-ion batteries are investigated. The results show that Fe_2O_3 has been fully reduced to Fe_3O_4 during the reduction. The Fe_3O_4 particles inherit the nano-size feature of Fe_2O_3 and are well dispersed in the composites. The composites with 60 and 70 wt.%AB additions possess a close capacity of ca. 430 mAh g^{-1} after 100 cycles, showing retentions of 85% and 95%, respectively. The Fe_3O_4/C composites converted from Fe_2O_3/AB mixtures show better electrochemical performance than the mixtures. The favorable electrochemical performance of the Fe_3O_4/C composites is mainly attributed to the homogeneous distribution of the Fe_3O_4 nanoparticles in the carbon matrix and the comparatively high electronic conductivity of Fe_3O_4. The synthesis method is suggested to be facile in large-scale production of superior anode materials for lithium-ion batteries.

1. Introduction

Lithium-ion secondary batteries are widely required in industrial and civil applications nowadays. However, the limited theoretical capacity of 372 mAh g^{-1} of the commercial anode material of graphite [1] cannot fully meet the requirement of high-energy density and high-power density of the power sources expected highly in electric vehicles, hybrid electric vehicles, power tools, the back-up for wind and solar energies, and so on. Novel anode materials with high performance are desired to replace the commercial one. Since Poizot et al. [2] reported that transition metal oxides of NiO, CoO, CuO and FeO could possess high capacities as anode materials for lithium-ion batteries (LIBs), a serious of transition metal oxides, including the above ones and Co_3O_4, Fe_2O_3 and Fe_3O_4, etc., have attracted intense attention [3–10] because of their high capacities of 2–3 times higher than that of graphite.

The electrochemical reaction mechanism of transition metal oxides with lithium is as the following [11]:

$$M_xO_y + 2ye^- + 2yLi^+ \leftrightarrow xM^0 + yLi_2O \quad (1)$$

where M = Fe, Co, Ni, Cu, etc. The transition metal oxides are reduced by lithium, leading to the formation of composite materials consisting of metallic clusters dispersed in an amorphous Li_2O matrix [2,12]. There is a large irreversible capacity caused by the formation of the solid electrolyte interface (SEI) and the partial irreversible lithium from the formation of Li_2O in the first discharge process. Severe aggregation and huge volume change of metal oxides also occur in the lithium insertion/extraction process, especially in the first cycle, which lead to poor cycle stability of the metal oxides.

* Corresponding authors. Tel./fax: 86 571 87952615.
E-mail addresses: gaomx@zju.edu.cn (M. Gao), honggepan@zju.edu.cn (H. Pan).

0378-7753/$ – see front matter © 2013 Elsevier B.V. All rights reserved.
http://dx.doi.org/10.1016/j.jpowsour.2013.03.073

Among those transition metal oxides, iron oxides of Fe_3O_4 and Fe_2O_3, which possess theoretical capacities of 926 [13] and 1005 mAh g^{-1} [14], respectively, are considered to be promising anode materials because of their advantages of high theoretical capacities, environmental benignity, high abundance, low cost, etc. [8–10,14,15]. As the high density of iron oxides (ca. 5.0 g cm^{-3}) compared to that of graphite (ca. 2.2 g cm^{-3}), the volumetric specific capacities of iron oxides are significant [16]. The discharge potential of iron oxide is higher than that of graphite, which reduces the potential safety problems with metallic lithium deposition on the host anode during rapid charge [17]. However, practical application of iron oxides as anode materials is still hindered by their poor cycling performance. In addition, the unsatisfied high-rate capability due to the comparatively low electron conductivity of iron oxides, especially for Fe_2O_3, is also a shortcoming.

Introducing carbonaceous materials into iron oxides, such as graphene [18,19], carbon nanotubes [20], carbon fibers [21], carbon coating [22] and carbon matrix [23,24], etc., shows useful actions in improving the cycle stability and also the rate capability of iron oxides. Carbonaceous materials can simultaneously buffer the volume change of the transformation between iron oxides and metallic iron during the discharge/charge process and increase the electronic contact of the iron oxides particles. Reducing the particles to nano-size [25–27] also plays effective roles in improving the electrochemical performance of iron oxides. Besides, special nano-architecture designs, such as coating Fe_3O_4 at Cu nanorods [28], flower-like Fe_3O_4 with carbon coating [29], carbon-coated Fe_3O_4 nanowires [30] and nanospindle [27], hollow nanoparticles [9,31], etc., are also found to be able to get favorable electrochemical performance. However, many preparation processes of high-performance iron oxides are extremely complicated and are of low yield. It is necessary to develop facile methods for large-scale production of iron oxides for anode materials of LIBs.

Compared to Fe_2O_3, Fe_3O_4 has higher electronic conductivity [10,28,32], which is favorable in improving cycle stability and rate capability. Therefore, in the present study, Fe_3O_4 is studied as anode material for LIBs. Acetylene black (AB), which possesses favorable electronic conductivity, being widely used as electronic conductive additive in both cathode and anode preparation of LIBs, is introduced to form Fe_3O_4/C composite anode materials. Commercial nano-Fe_2O_3 particles were ball-milled with AB in different weight ratios and subsequently followed by carbothermal reduction, conducting the formation of Fe_3O_4/C composites. As AB is also lithium-ion insertion/extraction active, the addition of AB not only improves the electronic contact of the Fe_3O_4 particles and buffers the volume change of Fe_3O_4 during cycling, but also contributes capacity to the electrode. The high electronic conductivity of AB is expected to maintain in the reduction products of Fe_3O_4/C composites. The structure change of the Fe_2O_3/AB mixtures during the carbothermal reduction and the electrochemical properties of the Fe_3O_4/C composites with different AB additions are investigated. The fabrication method is considered facile and of high yield. The result shows that the Fe_3O_4/C composite converted from Fe_2O_3/AB mixture by carbothermal reduction possesses favorable capacity and cycle stability.

2. Experimental

2.1. Synthesis and structure characterization

As-received α-Fe_2O_3 (Hangzhou Wanjing New Material Co., China) with size in the range of 30–120 nm were ball-milled on a planetary ball mill (QM–3SP4, Nanjing, China) with acetylene black (AB, Shanghai Haohua chemical Co., China) in weight ratios of 6/4, 5/5, 4/6 and 3/7 of Fe_2O_3 to AB, respectively, at 500 rpm for 15 h in acetone, forming slurries. The slurries were dried at 100 °C for 10 h to remove the acetone. The dried Fe_2O_3/AB mixtures were then carbothermally reduced at 600 °C for 6 h in flowing N_2, to obtain Fe_3O_4/C composites.

The crystalline phases of the composites were identified by X-ray diffraction (XRD, X-Pert Pro, Phillips) with a step interval of 0.02° and a count time of 1 s for per step, using Cu K_α radiation ($\lambda = 1.54$). The microstructure of the composites was observed by scanning electron microscopy (SEM, S-4800, Siron) and transmission electron microscopy (TEM, Tecnai G^2 F20). Fourier transform infrared spectrometry (FTIR, Bruker Tensor 27) analysis was used to identify the chemical bonds in the Fe_3O_4/C composite and Fe_2O_3/AB mixture in a transmission mode. The IR sample was prepared by cold pressing the tested material and potassium bromide (KBr), respectively.

2.2. Electrochemical characterization

The carbothermal reduced products were mixed with polyvinylidene fluoride (PVDF, Sinopec Shanghai Petrochemical Co., China) binder in a weight ratio of 8: 1 in 1-methyl-2-pyrrolidinone (NMP, No.5 Chemical Reagent Factory, Shanghai, China) solvent and then spreading onto Ni foam (Changsha Lyrun Material Co., China) to obtain electrodes. No additional electronic conductive additive was added. The electrodes were dried in a vacuum oven at 140 °C for 14 h and then pressed at a uniaxial pressure of 20 MPa to enhance the contact between the active material and Ni foam. The mass of the active material, including both the iron oxide and AB, on each anode was ca. 5 mg. Metallic lithium foil (Sinopharm Chemical Reagent Co., China) was used as reference and counter electrode. Coin cells of 2025 type were assembled in an argon-filled glove box (Labstar, Braun, Germany) with 1 M $LiPF_6$ in ethylene carbonate (EC)–dimethyl carbonate (DMC) (1:1 by volume) as electrolyte (Zhangjiagang Guotai Huarong New Chemical Materials Co., China) and a Celgard 2400 membrane was used as separator. Galvanostatic charge–discharge tests were performed at a constant discharge (lithiation) and charge (de-lithiation) current density of 100 mA g^{-1} in a potential range of 5 mV–3.0 V vs. Li^+/Li for the capacity and cycle stability of the composites by using a electrochemical test system (Neware Technology Co., China). Cyclic voltammetry (CV) tests were performed on an Arbin BT2000 system at a scanning rate of 0.1 mV s^{-1} at a potential window of 5 mV–3.0 V. Both the oxide and AB in the reduced product are taken as active material for the electrochemical property testing of the composites if it is not specially noticed. All of the electrochemical tests were performed at 25 ± 1 °C.

For comparison purpose, parallel experiments on selected structural characterization and electrochemical property testing of the ball-milled Fe_2O_3/AB mixtures as well as pure AB heat treated also at 600 °C for 6 h were also performed.

For further understanding the roles of AB and the conversion of Fe_2O_3 to Fe_3O_4 on the electrochemical performance of the composite anode materials, nominal electrochemical properties of only Fe_3O_4 in the composites as well as Fe_2O_3 in the ball-milled mixture are evaluated i.e., both the capacity of the electrode contributed nominally from AB and the mass of AB in the electrode are all subtracted. The details of the calculation are presented in electronic Supplementary information (ESI).

3. Results and discussion

3.1. Structure characterization

Fig. 1 shows the XRD patterns of the products converted from Fe_2O_3/AB mixtures with different AB additions by carbothermal

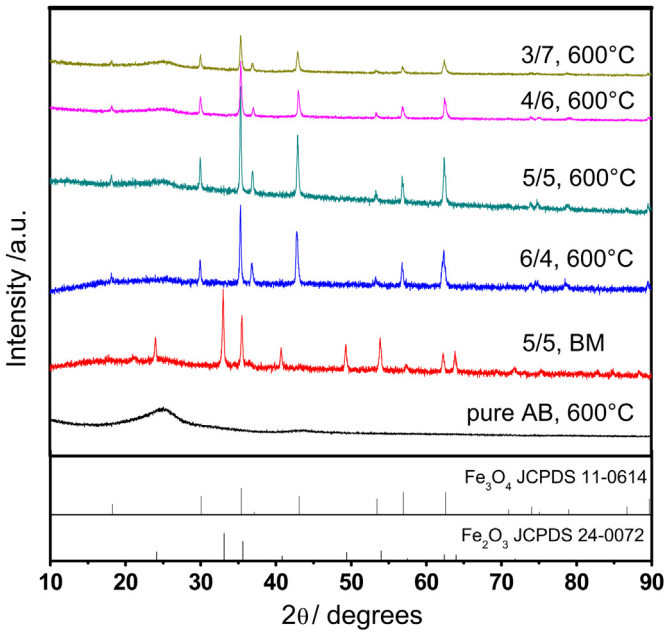

Fig. 1. XRD patterns of the products converted from Fe_2O_3/AB mixtures with weight ratios of Fe_2O_3 to AB of 6/4, 5/5, 4/6 and 7/3 by carbothermal reduction at 600 °C for 6 h, the ball milled (BM) mixture of Fe_2O_3/50 wt.%AB as well as AB heat-treated at 600 °C for 6 h.

reduction. For comparison, the patterns of the ball-milled mixture of Fe_2O_3/50 wt.%AB and the pure AB heat-treated are also shown. XRD analysis shows that the Fe_2O_3 in the ball-milled mixture was reduced to Fe_3O_4 (JCPDS 11-0614) after the carbothermal reduction. The plain AB shows a broad peak at around 25° after the heat treatment, indicating a common feature of poorly crystallized carbon as expected. The relative intensity of the peak of AB in the reduced product is greatly diminished due to its decreased content in the product. The crystallite sizes ((311) facet) of the Fe_3O_4 particles in the Fe_3O_4/C composites calculated by Scherrer formula [33] by using the XRD data decreases monotonously from ca. 39 nm–32 nm with the AB additions increase from 40 wt.% to 70 wt.%. However, the values are close to that of the original Fe_2O_3, ca. 35 nm, calculated also by Scherrer formula. If the conversion underwent such a reaction, $3Fe_2O_3 + C \rightarrow 2Fe_3O_4 + CO$, the weight ratios of Fe_3O_4 to C in the reduced product vary (increase) less than 2% compared to those of the initial Fe_2O_3 to AB. Therefore, the content of AB in the Fe_3O_4/C composite is taken as the same as that in its initial Fe_2O_3/AB mixture.

Fig. 2(a) shows a SEM micrograph of the as-received Fe_2O_3 particles. The as-received particles were severely agglomerated due to their high surface energy. After ball-milled with AB, the Fe_2O_3 particles were well dispersed in the mixture. The different amounts of AB additions don't cause evident change on the morphology feature of the Fe_2O_3/AB mixtures. A representative SEM micrograph of the as-milled Fe_2O_3/AB mixture is shown in Fig. 2(b), which is from the one with 60 wt.%AB addition. After the carbothermal reduction, there is also no visible morphology change compared with its original one. Fig. 2(c) shows a representative SEM micrograph of the Fe_3O_4/AB composites, which is converted from the Fe_2O_3/60wt.%AB mixture. As seen from Fig. 2(c), the Fe_3O_4 and AB particles are well dispersed to each other. The newly formed Fe_3O_4 particles inherit the nano-size feature of Fe_2O_3.

Fig. 3(a) and (b) shows the overall TEM micrographs of the Fe_3O_4/C composites converted from Fe_2O_3/AB with weight ratios of 6/4 and 4/6, respectively. The dark particles are Fe_3O_4, and the

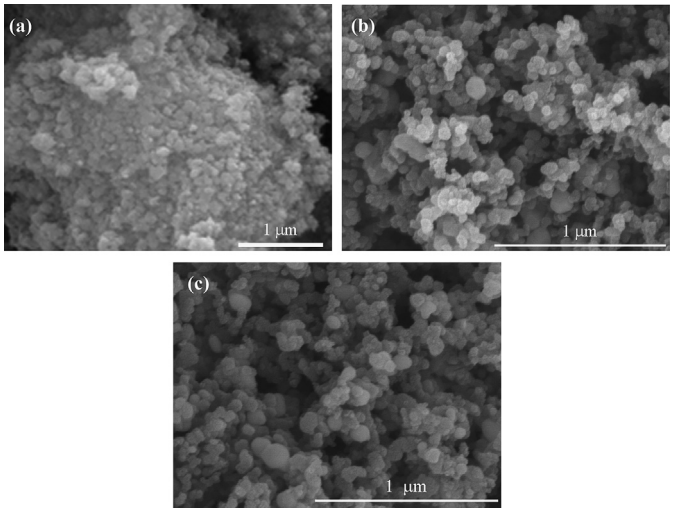

Fig. 2. SEM micrographs of the as-received Fe_2O_3 (a), the ball-milled mixture of Fe_2O_3/60wt.%AB (b), and the Fe_3O_4/C composite converted from Fe_2O_3/60wt.%AB (c).

smaller gray ones are AB particles. The AB particles maintain mostly their fine particle feature and most of them are connected with each other, forming a network. As seen from Fig. 3(a), for the composite converted from Fe_2O_3/40wt.%AB mixture, some of the Fe_3O_4 particles are surrounded by fine AB particles, but there are still considerable ones without the surrounding of AB particles. The Fe_3O_4 particles without AB particles surrounding are supposed to be mainly those originally having neighboring particles of Fe_3O_4. With increasing AB content to 60 wt.%, Fe_3O_4 particles are much fully surrounded by AB particles as seen from Fig. 3(b). Fig. 3(c) is a larger magnification TEM image of the Fe_3O_4/C composite with 60 wt.%AB addition. It is seen that Fe_3O_4 particles are well dispersed in AB particles and well contacted with AB particles.

In addition, FTIR analysis of the Fe_3O_4/C composite and Fe_2O_3/AB mixture (with 60 wt.%AB addition), the result of which is shown in Fig. S1 (ESI), shows that there is no chemical bond of C and O detected, indicating that the bonds of Fe_3O_4 or Fe_2O_3 and carbon in the Fe_3O_4/C composite or Fe_2O_3/AB mixture are physical ones.

3.2. Electrochemical properties

Fig. 4(a)–(d) shows the discharge/charge curves of the first and the following several cycles in the initial 10 ones of the Fe_3O_4/C

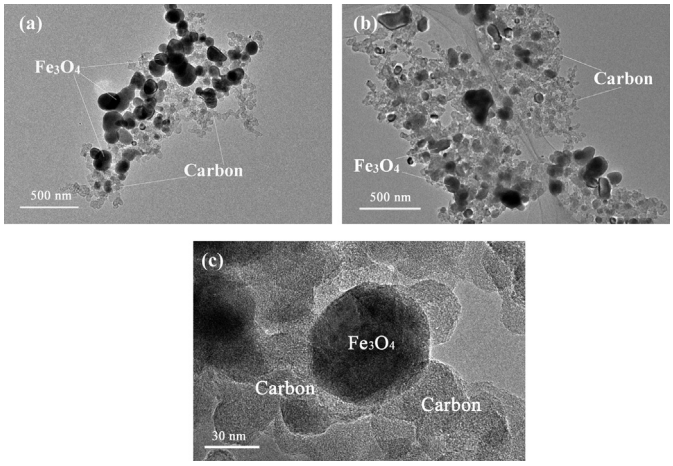

Fig. 3. Overall TEM micrographs of the Fe_3O_4/C composites with different AB additions: (a) 40 wt.%; (b) 60 wt.%, and a large magnification TEM image of Fe_3O_4/C with 60 wt.%AB addition (c).

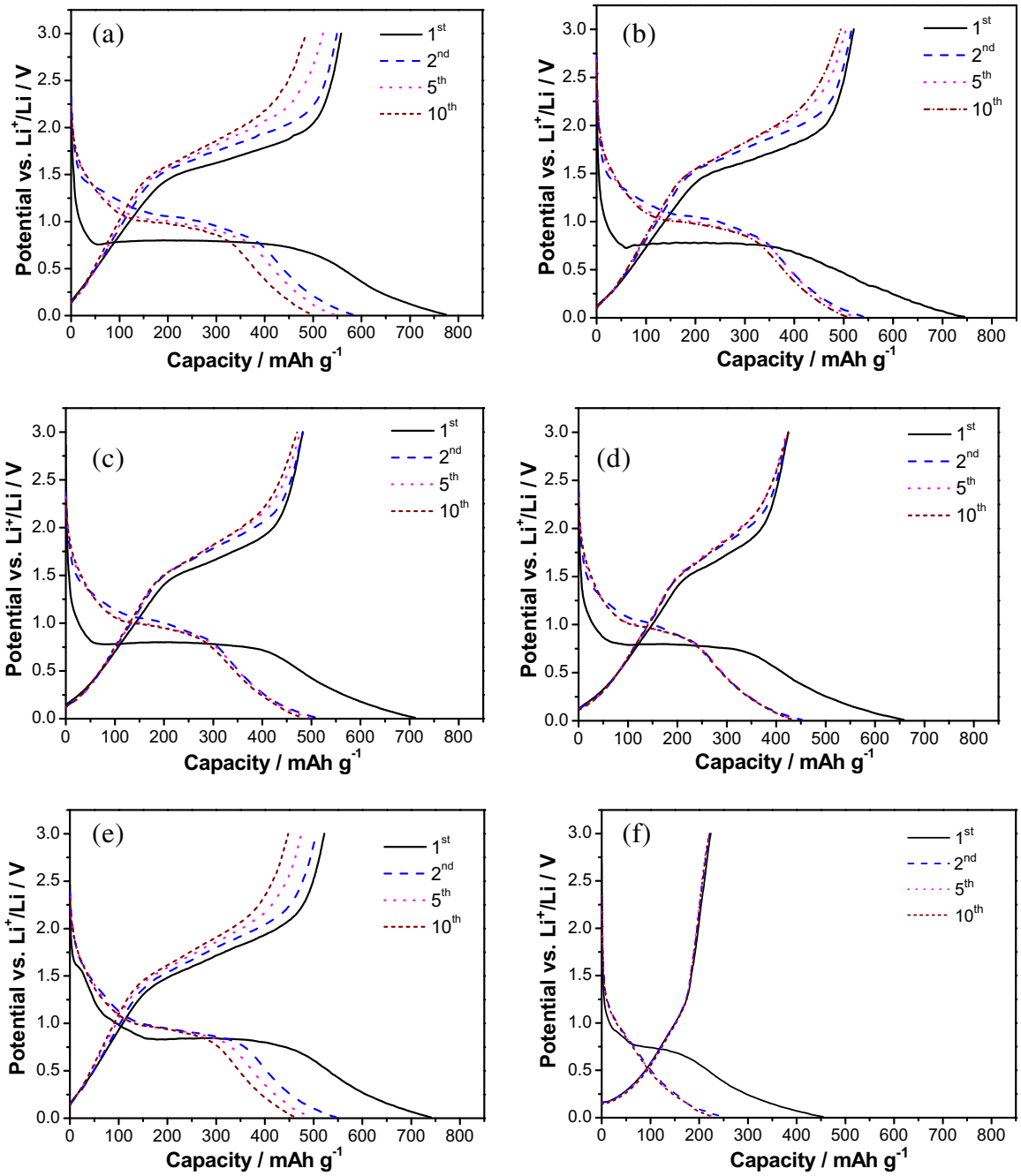

Fig. 4. The discharge/charge curves of the first and the following several cycles of the Fe_3O_4/C composites converted from Fe_2O_3/AB mixture with weight ratios of Fe_2O_3 to AB of 6/4 (a), 5/5 (b), 4/6 (c), 3/7 (d), and the ball milled mixture of Fe_2O_3/50 wt.%AB (e) as well as the heat-treated pure AB (f).

composites with different AB additions. For comparison, the curves of a selected ball-milled mixture of Fe_2O_3/50 wt.%AB as well as the heat-treated pure AB are also shown in Fig. 4(e) and (f), respectively. As seen from Fig. 4(a)–(d), large discharge plateaus around 0.8 V vs. Li^+/Li occur in all the Fe_3O_4/C samples, which are in accordance with the reduction of Fe_3O_4 by lithium reported in previous literature [15,20,25,27,34]. The gradual potential decay from ca. 0.8 V to the cut-off voltage corresponds to the lithium insertion (partial) in AB, as those did in other carbonaceous materials (such as the graphene [18], the citric acid derived carbon [35] and the carbon nanotubes [20], etc.), the decomposition of the electrolyte [15,18,36] and the partial formation of SEI layer on the surface of iron oxides [15,18]. In a α-Fe_2O_3 nanoflake system, it is reported that SEI layer on the surface of the Fe_2O_3 particles forms below the first discharge plateau of 0.75 V (vs. Li^+/Li) of the conversion reaction of Fe_2O_3 by lithium [15], and in a Fe_3O_4/graphene nanocomposite [18], the sloping curve from a similar first discharge plateau of 0.85 V to the cut-off potential is attributed to the formation of SEI layer and the reversible reaction between lithium and graphene sheets. Therefore, it may be obtained that the formation of SEI layer on the surface of Fe_3O_4 particles is at a lower potential than that of the reduction of Fe_3O_4 by lithium. Moreover, as reported by Larcher et al. [36], minor lithium insertion in Fe_2O_3 also exists in the early stage of the gradually dropped curve.

If it is checked carefully, the discharge potential plateau of the ball-milled mixture of Fe_2O_3/50wt%AB (Fig. 4(e)) is slightly higher

than those of the Fe_3O_4/C composites, indicating that the reduction of Fe_2O_3 in the Fe_2O_3/50wt%AB mixture by lithium is at a slightly higher potential than that of the Fe_3O_4 in the Fe_3O_4/C composites. Further comparing Fig. 4(a)–(d) with Fig. 4(e), it is found that there is only one steep and smooth slope in the potential range of 2.0–0.8 V in all the Fe_3O_4/C composites, which is very different from the Fe_2O_3/AB mixture that two slopes exist in this potential range, even for the sample with same AB addition. One slope correlating Fe_3O_4/C composites and two slopes correlating Fe_2O_3/C composites in the high discharge range are also reported by Zhang et al. [37]. However, two slopes in this high potential range also existed in nano-sized solid Fe_3O_4 [25,26] and carbon coated Fe_3O_4/C [29], and one slope feature was found in the micro-sized porous Fe_3O_4 [25] and solid Fe_2O_3 [26]. Generally, slopes at such high potential range during the discharge process are ascribed to lithium intercalation into bulk iron oxides [36] without destruction of the structure of iron oxides, forming $Li_xFe_3O_4$ [38] or $Li_xFe_2O_3$ [26] and $Li_2Fe_2O_3$ [36], before the conversion reaction of iron oxides to Fe and Li_2O. In a Fe_2O_3 system having two discharge slops in the high potential range reported by Larcher et al. [26], the comparatively higher-potential steep plateaus is supposed to attribute to the formation of α-$Li_xFe_2O_3$, and the relatively lower-potential steep plateaus is supposed to attribute to the formation of cublic-$Li_2Fe_2O_3$. The above information indicates that the lithium intercalation process of iron oxides does not simply depend on the type of iron oxides. Other factors such as size, textural and compositional characteristics of the materials also affect the characteristics of lithium intercalation in iron oxides.

With respect to the heat-treated pure AB, Fig. 4(f), there is a dropped plateau in the potential range of 0.95–0.75 V, which is suggested from the SEI formation. But the plateau is very limited as seen from Fig. 4(f). The SEI formation voltage on a carbonaceous (Li_xC_6) electrode in EC/DMC electrolyte is reported in the range of 0.6–1.5 V [39]. In addition, in a Fe_3O_4/SWNT (single-walled carbon nanotubes) system [20], it is proposed that the formation of SEI layer on the SWNTs takes place at around 1.0 V (vs. Li^+/Li), which is slightly higher than the discharge plateau of the conversion reaction of Fe_3O_4 to Fe. Therefore, it is suggested that the formation of SEI layer on the AB particles starts at slightly higher potential than that of the reduction of Fe_3O_4 by lithium. The following discharge plateau with slow drop and the subsequent comparatively rapid drop to the cut-off voltage are mainly attributed to the lithium intercalation in AB. However, SEI formation should also takes place continuously along the early stage of the discharge plateau. Moreover, the discharge plateau of AB is slightly lower than those of the Fe_3O_4/C composites as well as Fe_2O_3/50 wt.%AB mixture as seen from Fig. 4. Further more, the plateau of AB is not as flat as those of the iron oxides/C composites, indicating that lithium intercalates gradually in AB as the potential decreases, which is ascribed to the poor crystallinity nature of the AB.

In the charge process of the Fe_3O_4/C composites and the Fe_2O_3/AB mixture, the potential plateaus in the range of 1.4–2.0 V (vs. Li^+/Li) correspond to the oxidation of metallic Fe by Li_2O forming Fe_3O_4 for the Fe_3O_4/C composites and forming Fe_2O_3 for the Fe_2O_3/AB mixture, respectively. There is no visible plateau of lithium extraction in the charge process of pure AB, indicating a gradual extraction of lithium from Li_xC as the potential increases.

Further seen from Fig. 4(a)–(d), the discharge and charge curves of the Fe_3O_4/C composites develop to a much overlapped tendency after the first cycle, indicating an improvement in cycle stability. In addition, the redox transition of metallic Fe and Fe_3O_4/Fe_2O_3 moves to higher potentials (vs. Li^+/Li) in the second and the following cycles compared with those in the first cycle. The visible shift to high potential of the discharge process indicates a decreased resistance toward the reduction of the oxides, and the slight shift to high potential of the charge process is ascribed to polarization mainly.

The first discharge and charge capacities, the initial irreversible capacities and the initial coulombic efficiencies of the Fe_3O_4/C composites with different AB additions are listed in Table 1. For comparison, the corresponding values of the representative Fe_2O_3/AB mixture (with 50 wt.%AB addition) as well as pure AB (heat treated) are also listed. It is worth to note that, it is common that 10–15 wt.% electronic conductive additive, such as AB, super S carbon black, or other carbonaceous conductive additive, is added for anode preparation of powder materials. In most cases, such electronic conductive additive is not included in the mass of active materials when specific capacity of the anode materials is calculated, but the capacity (there is more or less some) contributed from those carbonaceous conductive additives is not subtracted from the tested capacity of the electrode. However, in the present study, no extra conductive additive was added, and both the AB and Fe_3O_4 in the composites were taken as active material, in this case, if the specific capacities (for either discharge or charge) of the present composites had been evaluated by the commonly used way mentioned above, the values should be at least 10% higher than the present reported values.

It is seen from Table 1, the first discharge capacities and the first reversible capacities of the Fe_3O_4/C composites decrease from 775 to 659 mAh g^{-1}, and from 612 to 453 mAh g^{-1}, respectively, with the AB additions increasing from 40 wt.% to 70 wt.%, which is mainly attributed to the lower capacity nature of AB. The initial irreversible capacities of the Fe_3O_4/C composites increase slightly from 218 to 234 mAh g^{-1} with the AB additions from 40 wt.% to 70 wt.%. As a result, the initial coulombic efficiencies of the Fe_3O_4/C composites decrease from 72% to 64% with the increase of the AB additions. The Fe_2O_3/50 wt.%AB mixture shows comparable values of first discharge capacity, initial coulombic efficiency and first reversible capacity to its converted Fe_3O_4/C. The heat-treated AB delivers a first discharge capacity of 454 mAh g^{-1} as seen in Table 1, but its initial coulombic efficiency is low, being of 49%, due to its large surface area which caused large areas of SEI layers, and hence more irreversible lithium intercalation. The initial coulombic efficiencies of the composites are not prominent, which is also due to the high surface area of the AB particles and also the nano-sized iron oxides (Fe_3O_4 and Fe_2O_3), which result in a large irreversible capacity from the formation of SEI layer on their surface.

Table 1
The electrochemical properties of the Fe_3O_4/C composites with different AB additions, the ball-milled mixture of Fe_2O_3/50 wt.%AB as well as the pure AB.[a]

Materials	1st discharge capacity/mAh g^{-1}	1st charge capacity/mAh g^{-1}	1st irreversible capacity/mAh g^{-1}	1st coulombic efficiency/%	1st reversible discharge capacity/mAh g^{-1}	100th discharge capacity/mAh g^{-1}	Capacity retention for 100 cycles/%
Fe_3O_4/C: 6/4	775 (990)	558(780)	218(210)	71.9(78.8)	612(853)	197(168)	32(20)
Fe_3O_4/C: 5/5	745 (1035)	521(817)	224(218)	69.9(79)	540(829)	331(421)	61(51)
Fe_3O_4/C: 4/6	712 (1098)	483(870)	229(227)	67.8(79.3)	511 (903)	433(711)	85(79)
Fe_3O_4/C: 3/7	659 (1136)	425(893)	234(243)	64.5(78.6)	453(924)	432(878)	95 (95)
Fe_2O_3/AB: 5/5	741 (1028)	522(820)	219 (208)	70.4(79.7)	546 (842)	273(304)	50(36)
Pure AB	454	224	230	49.3	250	241(241)	95

[a] Note: The values in the brackets are the corresponding nominal electrochemical properties of Fe_3O_4 in the Fe_3O_4/C composites and Fe_2O_3 in the Fe_2O_3/50 wt.%AB mixture.

Moreover, the values of the nominal corresponding electrochemical properties of only Fe_3O_4 in the composites and Fe_2O_3 in the representative Fe_2O_3/50 wt.%AB mixture calculated by Eq. S(1) (in ESI) are listed in the brackets in the corresponding columns in Table 1. The values listed in the brackets in Table 1 show that the nominal first discharge capacity of Fe_3O_4 in the composite increases from 990 to 1136 mAh g^{-1}, with the addition of AB from 40 wt.% to 70 wt.%. The Fe_3O_4 in the composites with different AB additions possesses a close nominal initial coulombic efficiency of 79%, which is higher than the initial coulombic efficiency of the Fe_3O_4/C composite as expected, as the negative effect on the initial coulombic efficiency caused by AB is roughly excluded. The nominal first discharge capacities of Fe_3O_4 in the composites with different AB additions are all higher than the theoretical value of Fe_3O_4 of 926 mAh g^{-1}. The excess capacities are attributed mainly to electrolyte reduction and subsequent the formation of an organic layer deposited at the surface of Fe_3O_4 particles, as occurred similarly at the nano-sized Fe_2O_3 particles reported by Larcher et al. [36], which was believed to occur in the 0.8 V region [36], and the formation of SEI layer at the surface of Fe_3O_4. The increasing nominal capacities in terms of the first discharge, first charge and initial reversible discharge of Fe_3O_4 in the composites indicate that a high content of AB addition in the composite favors either the reduction of Fe_3O_4 by lithium or the oxidation of Fe by Li_2O, which is supposed due to the enhanced electronic contact of the Fe_3O_4/Fe particles and the AB particles, as shown in Fig. 3(a) and (b) that a high AB content results in a much complete surrounding of AB particles to the Fe_3O_4 particles. In addition, the Fe_2O_3 in the Fe_2O_3/50 wt.%AB mixture shows comparable first discharge capacity, initial coulombic efficiency and initial reversible capacity to its converted Fe_3O_4 in the Fe_3O_4/C composite with same AB addition. However, considering the higher theoretic capacity of Fe_2O_3 compared to that of Fe_3O_4, it is obtained that the Fe_3O_4 in the composite possesses better lithium insertion and extraction performance than the Fe_2O_3 in the mixture.

Fig. 5(a)–(e) shows the CV curves of the Fe_3O_4/C composites with different AB additions as well as the ball-milled Fe_2O_3/50 wt.% AB mixture and the heat-treated pure AB. For the Fe_3O_4/C composites, there are evidently sharp reduction peaks at around 0.6 V in the first cathodic process, which are ascribed to the reduction of Fe_3O_4 by lithium forming metallic Fe and amorphous Li_2O, the electrolyte decomposition and the SEI formation [40,41] on the surfaces of both Fe_3O_4 and AB. In addition, as aforementioned, the SEI formation on the surface of AB particles starts at a higher potential than that on the surface of the Fe_3O_4 particles and also that of the reduction of Fe_3O_4 by lithium. Moreover, with the increasing amount of AB additions from 50 wt.% to 70 wt.%, the cathodic peak position moves slightly from 0.65 to 0.61 V.

For the Fe_2O_3/50wt%AB mixture, the first dominant cathodic peak of the formation of SEI layer (on the surfaces of both Fe_2O_3 and AB) and the reduction of Fe_2O_3 locates at a slightly higher potential of 0.67 V, which is in agreement with that found in the discharge curves (Fig. 4), that the discharge plateau of the Fe_2O_3/50 wt.%AB mixture is lightly higher than those of the Fe_3O_4/C composites. Besides, a weak cathodic peak occurs at 1.59 V. However, there is no such peak observed in the Fe_3O_4/C composites. The results are also consistent with those obtained in the discharge/charge curves of the samples (Fig. 4) that there are two steep slopes in the high potential range of 0.8–2.0 V for the Fe_2O_3/50wt%AB mixture, and there is only one slope in the same range for the Fe_3O_4/C composites. Weak cathodic peak at 1.6 V was also found at a porous Fe_2O_3 anode, which was ascribed to the formation of α-$Li_xFe_2O_3$ [42].

Fig. 5(e) shows the CV curve of pure AB (heat-treated). There is a cathodic peak located at 0.66 V (vs. Li^+/Li) in the first cycle, which is mainly ascribed to the formation of SEI layer. This peak almost disappeared in the subsequent cycles due to the formation of the SEI layer is irreversible. A comparison of Fig. 5(e) with Fig. 5(a)–(d) shows that the peak intensity of pure AB is much smaller than those of the Fe_3O_4/C composites and the Fe_2O_3/50 wt.%AB mixture. The comparison also shows that first cathodic peak of the SEI formation of AB is overlapped with the first cathodic peaks of the reduction of iron oxides by lithium of the Fe_3O_4/C composites and of the Fe_2O_3/50 wt.%AB mixture. Though the largest current of the SEI peak of AB is located at 0.66 V, as seen from Fig. 5(e), which is slightly higher than the positions at where the largest cathodic peaks of the Fe_3O_4/C composites located, however, as the current density of the SEI peak of AB is much smaller than those of the Fe_3O_4/C composites (Fig. 5(a)–(c)), it is obtained that the reduction of Fe_3O_4 by lithium contributed mainly to the cathodic peak of the composites. Moreover, the slightly lowered potential of the cathodic peak of the composite from 0.65 to 0.61 V with the increase of the AB addition is probably due to the slight crystalline structure change of the reduced crystallite size of Fe_3O_4 particles with the increase of AB additions as aforementioned. However, the variations of the cathodic peak positions are very limited, and there are no visible changes on the discharge plateaus of the Fe_3O_4/C composites with the different AB additions. In addition, as further seen in Fig. 5, lithium intercalations in the present AB of either pure AB or in Fe_3O_4/C composites and Fe_2O_3/AB mixture took place gradually as the potential decreased.

There are two anodic peaks in the first cycle of both the Fe_3O_4/C composites and the Fe_2O_3/AB mixture, which locate at ca. 1.6–1.7 and 1.8–1.9 V, respectively. This means that the oxidation of metallic Fe by Li_2O to Fe_3O_4 or Fe_2O_3 takes place by two steps. Two anodic peaks at 1.6/1.9 V and 1.75/1.9 V were also found in hollow Fe_3O_4 microspheres [43] and Fe_3O_4/C nanorods [22], respectively, which were suggested to correspond to the oxidation of Fe^0 to Fe^{2+} and partly to Fe^{3+}, respectively. Further seen from Fig. 5(a)–(c), for the Fe_3O_4/C composites, the intensity and the integral area of the low-potential peak are slightly larger than those of the high-potential ones, indicating an insufficient oxidation process for the latter. Whereas for the Fe_2O_3/AB mixture (Fig. 5(d)), the difference in the intensity and the integral area between the two anodic peaks is not visible, indicating a comparable oxidation process at the different potentials.

There is a visible anodic peak at ca. 0.3 V in the first cycle of pure AB (Fig. 5(e)), which is ascribed to lithium extraction from Li_xC. Lithium extraction from Li_xC is reported at 0.2 V by Mi et al. [44]. The present potential of lithium extraction from Li_xC is slightly higher, which is probably due to the different type of carbon from that reported. A wide anodic peak at ca. 0.2 V is also observed in the CV curves of the Fe_3O_4/C composites and Fe_2O_3/AB mixture (Fig. 5(a)–(d)), which is slightly lower than that of pure AB, indicating the resistance of lithium extraction from Li_xC in the Fe_3O_4/C composites and Fe_2O_3/AB mixture is lower.

In the subsequent second cycles, the main cathodic peaks of the Fe_3O_4/C composites and the Fe_2O_3/AB mixture all move to higher potentials, and split into two peaks (ca. 0.8/0.9 V), as seen in Fig. 5(a)–(d). The split two cathodic peaks indicate that the reduction of Fe_3O_4/Fe_2O_3 to metallic Fe by lithium was conducted by two steps. Similar phenomenon is also found in Fe_2O_3/C electrode [44]. In addition, the peak current and the integrated area are evidently reduced compared to those of the initial ones, indicating a decreased capacity in the second cycle. As the formation of Li_2O and Fe from the reduction of iron oxide by lithium is thermodynamically feasible and the extraction of Li from Li_2O is thermodynamically impossible [45], capacity loss exists inevitably in the first charge process due to the incomplete transformation of metallic Fe to iron oxide by reacting with Li_2O formed in the first discharge process, and hence results in inevitable loss of active material of

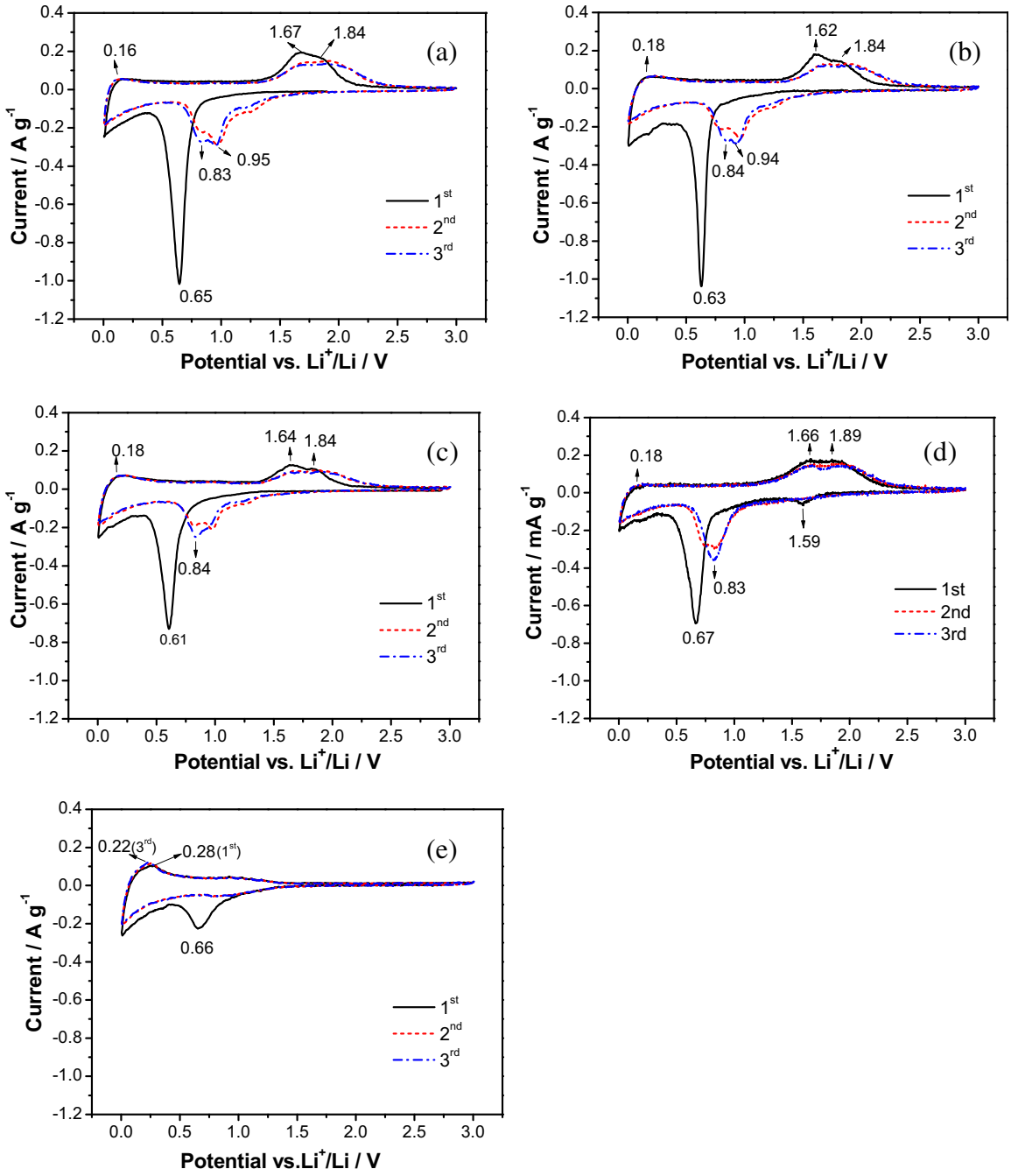

Fig. 5. CV curves of the first three cycles of the Fe_3O_4/C composites converted from Fe_2O_3/AB with weight ratios of Fe_2O_3 to AB of 5/5 (a), 4/6 (b), 3/7 (c), and the ball-milled mixture of Fe_2O_3/50wt%AB (d) as well as the heat-treated pure AB (e).

iron oxide after the first cycle. In addition, both the cathodic peaks and the anodic peaks of the Fe_3O_4/C composites and Fe_2O_3/AB mixture in the second cycle shift to higher potential positions compared to those in the first cycle, which are consistent with those obtained from their discharge and charge curves (Fig. 4(a)–(e)). The significant difference in the potential (vs. Li^+/Li) of the cathodic peaks in the second cycle from that in the first cycle is due to the structure modification of the iron oxides [46] and also the strain introduced in the iron oxides during the first cycle caused by the lithium insertion and extraction. The shift of the anodic peaks to high potential after the first cycle is ascribed to the polarization as usual [47]. However, since the second cycle, the reversibility is improved, as seen in the CV curves of the 2nd and 3rd cycles, due to the similar structure and strain of the active materials. Because of the hysteresis in the CV technique [48], the cathodic peak shift to a lower potential, and the anodic peak shifts to a higher potential compared to the discharge/charge plateaus obtained from the discharge/charge curves (Fig. 4).

The cycling performance of the Fe_3O_4/C composites converted from Fe_2O_3/AB mixture with different AB contents is shown in Fig. 6(a). For comparison, the values of the as-milled mixture of Fe_2O_3/50 wt.%AB and the heat-treated pure AB are also shown. The capacities and capacity retentions of the Fe_3O_4/C composites, the Fe_2O_3/50 wt.%AB mixture as well as the pure AB after 100 cycles are

also listed in Table 1. In addition, the nominal capacities and capacity retentions of Fe_3O_4 in the Fe_3O_4/C composites and Fe_2O_3 in the Fe_2O_3/50 wt.%AB mixture after 100 cycle calculated by Eq. S(1) are also listed in the brackets of the corresponding columns in Table 1. As shown in Fig. 6(a) and Table 1, though pure AB possesses a large irreversible capacity in the first cycle, it retains a high cycle stability in the subsequent cycles. The cycle stability of the Fe_3O_4/C composites increases with the addition of AB. The specific capacities of the Fe_3O_4/C composites with 60 wt.% and 70 wt.%AB additions reach a close value of ca. 430 mAh g^{-1} after 100 cycles, possessing capacity retentions as high as 85% and 95%, respectively. However, the capacity retentions of the Fe_3O_4/C composites with 50 wt.% and 40 wt.%AB additions are only of 61% and 32%, respectively, and the capacities are only of 331 and 197 mAh g^{-1}, after 100 cycles. It is obtained that a relatively large content of AB is necessary for this type of electrode. The much full surrounding of AB particles to the Fe_3O_4 particles in the Fe_3O_4/C composites with higher AB addition (Fig. 3(a) and (b)) provides enhanced electronic contacting of the Fe_3O_4 particles, favoring the cycle stability. In addition, sufficient amount of AB prevents effectively the agglomeration of Fe_3O_4 and accommodates the large volume expansion/shrinkage of Fe_3O_4 and also avoids crack and pulverization of the electrode, therefore preserves the integrities of the electrodes during continuous charging/discharging.

Moreover, the Fe_3O_4/C composites converted from Fe_2O_3/AB mixtures with various AB additions all show better overall capacity performance than the Fe_2O_3/AB mixtures during cycling, as from the comparison with the cycle performance of the Fe_2O_3/AB mixtures in 100 cycles shown in Fig. S2 with Fig. 6(a). For example, though the first discharge capacity, the first discharge capacity and the first reversible capacity of the ball-milled Fe_2O_3/50 wt.%AB mixture are comparable to those of its converted Fe_3O_4/C composite (Table 1 and Fig. 6(a)), the discharge capacity of 331 mAh g^{-1} of the Fe_3O_4/C composite after 100 cycles is much higher than that of 243 mAh g^{-1} of the Fe_2O_3/50 wt.%AB mixture. The capacity retention of 61% of the Fe_3O_4/C composite converted from Fe_2O_3/50 wt.%AB after 100 cycles is also much higher than that of the Fe_2O_3/50 wt.%AB, 50%. The higher electronic conductivity of Fe_3O_4 compared to that of Fe_2O_3 is supposed to be one of the important factors for the better electrochemical performance of the Fe_3O_4/C composites. In addition, the contact of the Fe_3O_4 and AB particles might also be improved during the carbothermal reduction process, which also favors the electrochemical properties of the Fe_3O_4/C composites.

The nominal cycle performance of Fe_3O_4 in the Fe_3O_4/C composites as well as Fe_2O_3 in the Fe_2O_3/50 wt.%AB mixture is shown in Fig. 6(b). It is seen that the Fe_3O_4 in the Fe_3O_4/C composites with higher AB addition not only possesses higher cycle stability, but also higher capacity. This means that a higher content of AB addition helps to conduct much complete lithium insertion and extraction in the transformation of $Fe_3O_4 \leftrightarrow Fe$ during cycling. In addition, the Fe_2O_3 in the mixture of Fe_2O_3/50 wt.%AB mixture still shows lower nominal capacity and capacity retention compare to its converted Fe_3O_4 in the Fe_3O_4/C composite.

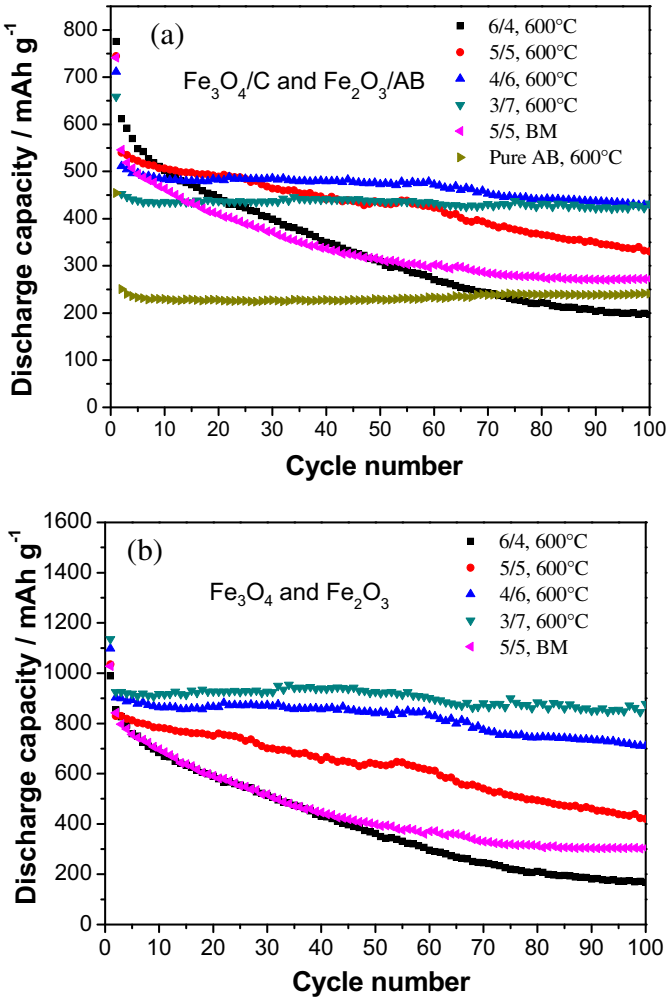

Fig. 6. Cycling performance of the Fe_3O_4/C composites converted from Fe_2O_3/AB with weight ratios of Fe_2O_3 to AB of 6/4, 5/5, 4/6, 3/7, as well as the ball-milled Fe_2O_3/50 wt.%AB mixture and the heat-treated pure AB (a), and the nominal cycle performance of Fe_3O_4 in the Fe_3O_4/C composites as well as Fe_2O_3 in the Fe_2O_3/50 wt.%AB mixture (b).

4. Conclusions

Fe_3O_4/C composites are successfully prepared by a quite facile carbothermal reduction of the ball-milled mixtures of nano-sized Fe_2O_3 and acetylene black (AB). The Fe_3O_4 particles inherit the nano-size feature of the Fe_2O_3 particles and are well dispersed in the composites. The Fe_3O_4/C composites converted from Fe_2O_3/AB mixtures with various AB additions all possess better overall capacity and capacity retention performance compared to the Fe_2O_3/AB mixtures during cycling, which is attributed to the comparatively higher electronic conductivity of Fe_3O_4 compared to Fe_2O_3 and also probably due to the improved contact of the Fe_3O_4 and AB particles due to the carbothermal reduction treatment. Sufficient AB is necessary for this anode material to tolerate the volume change of the Fe_3O_4 particles and to preserve an effective electric-contacted network to the Fe_3O_4 particles. The Fe_3O_4/C composites with 60 and 70 wt.%AB additions possess a similar capacity of 430 mAh g^{-1} and show retentions of 85% and 95%, respectively, after 100 cycles. A higher content of AB addition helps to conduct a much complete lithium insertion and extraction in the transformation of Fe_3O_4 and Fe during cycling. The increase of AB content not only favors the cycle stability, but also favors the capacity of Fe_3O_4 itself. The present synthesis method is attractive for large-scale production of superior anode materials for LIBs.

Acknowledgments

This work was supported by National Nature Science Foundation for Distinguished Youth Scholars of China (No. 51025102) and the Key Science and Technology Innovation Team of Zhejiang Province, PR China (No. 2010R50013).

Appendix A. Supplementary data

Supplementary data related to this article can be found online at http://dx.doi.org/10.1016/j.jpowsour.2013.03.073.

References

[1] R. Fong, U. Vonsacken, J.R. Dahn, Journal of the Electrochemical Society 137 (1990) 2009–2013.
[2] P. Poizot, S. Laruelle, S. Grugeon, L. Dupont, J.M. Tarascon, Nature 407 (2000) 496–499.
[3] J. Zhong, X.L. Wang, X.H. Xia, C.D. Gu, J.Y. Xiang, J. Zhang, J.P. Tu, Journal of Alloys and Compounds 9 (2011) 3889–3893.
[4] L.B. Chen, N. Lu, C.M. Xu, H.C. Yu, T.H. Wang, Electrochimica Acta 54 (2009) 4198–4201.
[5] F.Y. Cheng, Z.L. Tao, J. Liang, J. Chen, Chemistry of Materials 20 (2008) 667–681.
[6] P. Zhang, Z.P. Guo, Y.D. Huang, D.Z. Jia, H.K. Liu, Journal of Power Sources 196 (2011) 6987–6991.
[7] L. Tian, H.L. Zhou, J.X. Fu, X.F. Yang, Y. Wang, H.L. Guo, X.H. Fu, C.L. Liang, M.M. Wu, P.K. Shen, Q.M. Gao, Advanced Functional Materials 20 (2010) 617–623.
[8] M. Zhang, B.H. Qu, D.N. Lei, Y.J. Chen, X.Z. Yu, L.B. Chen, Q.H. Li, Y.G. Wang, T.H. Wang, Journal of Materials Chemistry 22 (2012) 3868–3874.
[9] Z.Y. Wang, L. Zhou, X.W. Lou, Advanced Materials 24 (2012) 1903–1911.
[10] S.K. Behera, Journal of Power Sources 196 (2011) 8669–8674.
[11] J. Li, H.M. Dahn, L.J. Krause, D.B. Le, J.R. Dahn, Journal of the Electrochemical Society 155 (2008) A812–A816.
[12] Y.M. Kang, M.S. Song, J.H. Kim, H.S. Kim, M.S. Park, J.Y. Lee, H.K. Liu, S.X. Dou, Electrochimica Acta 50 (2005) 3667–3673.
[13] X.Y. Zhao, D.G. Xia, K. Zheng, Journal of Alloys and Compounds 513 (2012) 460–465.
[14] M. Du, C.H. Xu, J. Sun, L. Gao, Electrochimica Acta 80 (2012) 302–307.
[15] M.V. Reddy, T. Yu, C.H. Sow, Z.X. Shen, C.T. Lim, G.V.S. Rao, B.V.R. Chowdari, Advanced Functional Materials 17 (2007) 2792–2799.
[16] P.C. Wang, H.P. Ding, Tursun Bark, C.H. Chen, Electrochimica Acta 52 (2007) 6650–6655.
[17] J.M. Tarascon, M. Armand, Nature 414 (2001) 359–367.
[18] P.C. Lian, X.F. Zhu, H.F. Xiang, Z. Li, W.S. Yang, H.H. Wang, Electrochimica Acta 56 (2010) 834–840.
[19] W. Shi, J.X. Zhu, D.H. Sim, Y.Y. Tay, Z.Y. Lu, X.J. Zhang, Y. Sharma, M. Srinivasan, H. Zhang, H.H. Hng, Q.Y. Yan, Journal of Materials Chemistry 21 (2011) 3422–3427.
[20] C.M. Ban, Z.C. Wu, D.T. Gillaspie, L. Chen, Y.F. Yan, J.L. Blackburn, A.C. Dillon, Advanced Materials 22 (2010) E145–E149.
[21] S.W. Han, D.W. Jung, J.H. Jeong, E.S. Oh, Journal of Applied Electrochemistry 42 (2012) 1057–1064.
[22] Q.Q. Xiong, Y. Lu, X.L. Wang, C.D. Gu, Y.Q. Qiao, J.P. Tu, Journal of Alloys and Compounds 536 (2012) 219–225.
[23] M. Nagao, M. Otani, H. Tomita, S. Kanzaki, A. Yamada, R. Kanno, Journal of Power Sources 196 (2011) 4741–4746.
[24] B.T. Hang, I. Watanabe, T. Doi, S. Okada, J. Yamaki, Journal of Power Sources 161 (2006) 1281–1287.
[25] Y.X. Chen, L.H. He, P.J. Shang, Q.L. Tang, Z.Q. Liu, H.B. Liu, L.P. Zhou, Journal of Materials Science and Technology 27 (2011) 41–45.
[26] D. Larcher, C. Masquelier, D. Bonnin, Y. Chabre, V. Masson, J.B. Leriche, J.M. Tarascon, Journal of the Electrochemical Society 150 (2003) A133–A139.
[27] W.M. Zhang, X.L. Wu, J.S. Hu, Y.G. Guo, L.J. Wan, Advanced Functional Materials 18 (2008) 3941–3946.
[28] P.L. Taberna, S. Mitra, P. Poizot, P. Simon, J.M. Tarascon, Nature Materials 5 (2006) 567–573.
[29] S.L. Jin, H.G. Deng, D.H. Long, X.J. Liu, L. Zhan, X.Y. Liang, W.M. Qiao, L.C. Ling, Journal of Power Sources 196 (2011) 3887–3893.
[30] T. Muraliganth, A.V. Murugan, A. Manthiram, Chemical Communications 47 (2009) 7360–7362.
[31] B. Koo, H. Xiong, M.D. Stater, V.B. Prakapenka, M. Baasubramanian, P. Podsiadlo, C.S. Johnson, T. Rajh, E.V. Shevchenko, Nano Letters 12 (2012) 2429–2435.
[32] J.P. Liu, Y.Y. Li, H.J. Fan, Z.H. Zhu, J. Jiang, R.M. Ding, Y.Y. Hu, X.T. Huang, Chemistry of Materials 22 (2010) 212–217.
[33] H.P. Klug, L.E. Alexander, X-ray Diffraction Procedures for Polycrystalline and Amorphous Materials, Wiley, New York, 1974, p. 618.
[34] Y. He, L. Huang, J.S. Cai, X.M. Zheng, S.G. Sun, Electrochimica Acta 55 (2010) 1140–1144.
[35] M.X. Gao, X. Chen, H.G. Pan, L.S. Xiang, F. Wu, Y.F. Liu, Electrochimica Acta 55 (2010) 9067–9074.
[36] D. Larcher, D. Bonnin, R. Cortes, I. Rivals, L. Personnaz, J.M. Tarascon, Journal of the Electrochemical Society 150 (2003) A1643–A1650.
[37] M. Zhang, X.M. Yin, Z.F. Du, S. Liu, L.B. Chen, Q.H. Li, H. Jin, K. Peng, T.H. Wang, Solid State Sciences 12 (2010) 2024–2029.
[38] L. Chun, X.Z. Wu, X.M. Lou, Y.X. Zhang, Electrochimica Acta 55 (2010) 3089–3092.
[39] P.B. Balbuena, Y.X. Wang, Lithium-ion Batteries, Solid–Electrolyte Interphase, Imperial College Press, 2004, p. 5.
[40] Y.Z. Piao, H.S. Kim, Y.E. Sung, T. Hyeon, Chemical Communications 46 (2010) 118–120.
[41] G. Zhou, D.W. Wang, F. Li, L. Zhang, N. Li, Z.S. Wu, L. Wen, G.Q. Lu, H.M. Cheng, Chemistry of Materials 22 (2010) 5306–5313.
[42] D.W. Su, H.S. Kim, W.S. Kim, G.X. Wang, Microporous and Mesoporous Materials 149 (2012) 36–45.
[43] H.S. Lim, B.Y. Jung, Y.K. Sun, K.D. Suh, Electrochimica Acta 75 (2012) 123–130.
[44] H.Y. Mi, Y.L. Xu, W. Shi, H.D. Yoo, O.B. Chae, S.M. Oh, Materials Research Bulletin 47 (2012) 152–155.
[45] J. Chen, L.N. Xu, W.Y. Li, X.L. Gou, Advanced Materials 17 (2005) 584–586.
[46] M.Y. Li, Y. Wang, C.L. Liu, H. Gao, W.S. Dong, Electrochimica Acta 67 (2012) 187–193.
[47] L.W. Ji, Z.K. Tan, T.R. Kuykendall, S. Aloni, S. Xun, E. Lin, V. Battaglia, Y.G. Zhang, Physical Chemistry Chemical Physics 13 (2011) 7139–7146.
[48] H. Liu, G.X. Wang, J.Z. Wang, D. Wexler, Electrochemistry Communications 10 (2008) 1879–1882.